# Dynamic Nuclear Polarization with Single Electron Spins

J. R. Petta,[1,2] J. M. Taylor,[1,3] A. C. Johnson,[1] A. Yacoby,[1] M. D. Lukin,[1] C. M. Marcus,[1] M. P. Hanson,[4] and A. C. Gossard[4]

[1]*Department of Physics, Harvard University, 17 Oxford St., Cambridge, Massachusetts 02138, USA*
[2]*Department of Physics, Princeton University, Princeton, New Jersey 08544, USA*
[3]*Department of Physics, Massachusetts Institute of Technology, Cambridge, Massachusetts 02139, USA*
[4]*Materials Department, University of California, Santa Barbara, California 93106, USA*

We polarize nuclear spins in a GaAs double quantum dot by controlling two-electron spin states near the anticrossing of the singlet ($S$) and $m_S = +1$ triplet ($T_+$) using pulsed gates. An initialized $S$ state is cyclically brought into resonance with the $T_+$ state, where hyperfine fields drive rapid rotations between $S$ and $T_+$, "flipping" an electron spin and "flopping" a nuclear spin. The resulting Overhauser field approaches 80 mT, in agreement with a simple rate-equation model. A self-limiting pulse sequence is developed that allows the steady-state nuclear polarization to be set using a gate voltage.

Semiconductor quantum dots share many features with real atoms: they possess discrete electronic energy states, obey Hund's rules as the states are filled, and can be coupled to one another, creating artificial molecules [1,2]. In contrast to atoms, where electrons are coupled to a single nucleus, electrons within quantum dots interact with many (typically $\sim 10^6$) lattice nuclei [2]. The dynamics of spin systems comprising few electrons interacting with many nuclei is an interesting and complex many-body problem in condensed matter physics [3–6].

Electrically controlled nuclear polarization has been investigated in gate-defined quantum point contacts (QPCs) in GaAs, where nuclear polarization driven by scattering between spin-polarized edge states induced hysteresis in conductance as a function of magnetic field [7,8]. In few-electron quantum dots, transport in the so-called Pauli blockade regime, which requires a spin flip for conduction, can exhibit long time scale oscillations and bistability, also understood to result from a buildup and relaxation of nuclear polarization during spin-flip-mediated transport [6,9–11]. Sizable polarizations can result from transport in this regime [12]. Spin relaxation at low magnetic fields (time scale $T_1$) and spin dephasing (time scale $T_2^*$) in GaAs double quantum dots are limited by hyperfine interactions with host nuclei [13–17]. Theory suggests that electron spin dephasing times may be extended by cooling nuclear spins through nuclear polarization and projective measurement [6,18,19]. In addition, nuclear spins may be used as a quantum memory due to long nuclear spin coherence times [20]. For these reasons, it is desirable to have the ability to control interactions between a *single* confined electron spin and a bath of quantum dot nuclear spins [21].

In this Letter, we use fast pulsed-gate control of two-electron spin states in a double quantum dot to create and detect nuclear polarization. Rather than using spin-flip-mediated transport with an applied bias [11,12], we use a cycle of gate voltages to prepare a spin singlet ($S$) state,

induce nuclear flip-flop at the singlet-triplet ($S$-$T_+$) anticrossing, and measure the resulting nuclear polarization from the position of that anticrossing. In this way, dynamic nuclear polarization (DNP) is achieved (and measured) by the controlled flipping of single electron spins. Additionally, we demonstrate a self-limiting pulse cycle with fixed period that allows voltage-controlled "programming" of steady-state nuclear polarization. Experimental results are found to be in qualitative agreement with a simple rate-equation model.

Measurements are carried out using a gated-defined GaAs double quantum dot configured near the (1,1)-(0,2) charge transition [see Fig. 1(a)] [14]. A QPC charge sensor is used to read out the time-averaged charge configuration of the dot, from which spin states can be inferred. Relevant energies of spin states as a function of detuning, $\epsilon \propto V_R - V_L$, are shown in Fig. 1(b). The (1,1) singlet, $S$, and (0,2) singlet, denoted $(0, 2)S$, hybridize near $\epsilon = 0$ due to interdot tunneling. Triplets of (0,2) are not considered, due to the large singlet-triplet splitting, $E_{ST} \sim 400$ $\mu$eV. The triplet states of (1,1), $T_+$, $T_-$, and $T_0$ do not hybridize with $(0, 2)S$ due to spin selection rules. An external magnetic field, $\vec{B}_0$, applied perpendicular to the plane of the two-dimensional electron gas (2DEG), adds to the hyperfine field, $\vec{B}_{nuc}$, resulting in a total effective Zeeman field $\vec{B}_{tot} = \vec{B}_0 + \vec{B}_{nuc}$. The Zeeman energy, $E_Z = g^* \mu_B B_{tot}$, lifts the triplet-state degeneracy, where $B_{tot} = |\vec{B}_{tot}|$ and $g^* \sim -0.4$ are the effective electronic $g$-factor in GaAs. The nuclear Zeeman field is proportional to nuclear polarization and has a magnitude $|\vec{B}_{nuc}| = 5.2$ T for fully polarized nuclei in GaAs [22].

Hyperfine fields rapidly drive transitions between $S$ and $T_0$ on a 10 ns time scale at large negative detuning, where these states become degenerate [10,14]. However, these transitions do not polarize nuclei since $\Delta m_S = 0$. In contrast, a transition from $S$ to $T_+$ flips an electron spin, $\Delta m_S = 1$. When driven by the hyperfine interaction, this
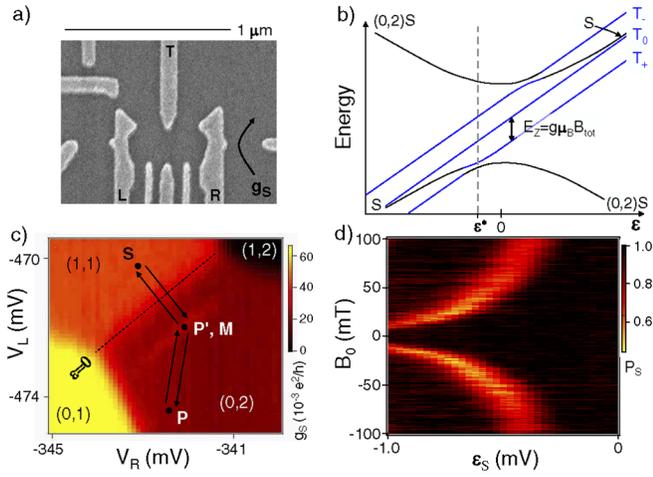
a)



b)



c)



d)



FIG. 1 (color online). (a) SEM image of a device similar to the one used in this experiment. A QPC with conductance, $g_S$, senses charge on the double dot. (b) Energy levels near the (1,1)-(0,2) charge transition. (c) $g_S$ measured as a function of $V_L$ and $V_R$. A pulse sequence used to polarize nuclei is superimposed on the charge stability diagram (see text). The bright signal at point $M$ that runs parallel to the $\epsilon = 0$ line is a result of Pauli-blocked $(1, 1) \rightarrow (0, 2)$ charge transitions and reflects $S$-$T_+$ mixing at point $S$. (d) $P_S(\tau_S = 200 \text{ ns})$ as a function of $\epsilon_S$ and $B_0$. The field dependent "spin funnel" corresponds to the $S$-$T_+$ anticrossing position, $\epsilon_S = \epsilon^*$.

electron spin "flip" is accompanied by a nuclear spin "flop" with $\Delta m_I = -1$. The change in $B_{\text{nuc}}$ associated with this flip-flop transition is along the direction of external field, taking into account the positive nuclear $g$ factors for Ga and As [2]. The cyclic repetition of the transition from $S$ to $T_+$ can thereby lead to a finite time-averaged $B_{\text{nuc}}$ oriented along the external field.

The value of detuning where the $S$-$T_+$ anticrossing occurs, denoted $\epsilon^*$ [see Fig. 1(b)], is a sensitive function of $B_{\text{tot}}$ for $|B_{\text{tot}}| \lesssim 80$ mT, providing a straightforward means of measuring $B_{\text{nuc}}$ within that range. To calibrate the measurement, the dependence of $\epsilon^*$ on external field amplitude $B_0$ is measured using the pulse sequence shown in Fig. 1(c): The $(0, 2)S$ state is first prepared at point $P$. A delocalized singlet in (1,1) is created by moving to point $S$ (detuning $\epsilon_S$) via point $P'$. The system is held at point $S$ for a time $\tau_S \gg T_2^*$ then moved to point $M$ and held there for the longest part of the cycle. The sequence is then repeated. When $\epsilon_S = \epsilon^*$, rapid mixing of $S$ and $T_+$ states occurs. When the system is moved to point $M$, the (1,1) charge state will return to (0,2) only if the separated spins are in a singlet configuration. The probability of being in the singlet state after time $\tau_S$ thus appears as charge signal—the difference between the (1,1) and (0,2) charge states—detected by measuring the time-averaged QPC conductance, $g_S$ [see Fig. 1(a)]. Figure 1(c) shows $g_S$ as a function of $V_L$ and $V_R$ with this pulse sequence applied. The field dependence of this signal is shown in Fig. 1(d), which plots the calibrated singlet state probability, $P_S$, as a function of

$B_0$ and $\epsilon_S$. In Fig. 1(d), $P_S \sim 0.7$ at the $S$-$T_+$ degeneracy, corresponding to a probability of electron-nuclear flip-flop per cycle $(1 - P_S) \sim 0.3$. The position of the anticrossing, $\epsilon_S = \epsilon^*$, becomes more negative as $B_0$ decreases toward zero [Fig. 1(d)], as expected from the level diagram, Fig. 1(b).

An alternative sequence that (in principle) deterministically flips one nuclear spin per cycle and allows greater control of the steady-state nuclear polarization is shown in Fig. 2(b): In this case, the initial $(0, 2)S$ is separated quickly ($\sim 1$ ns), to a value of detuning beyond the $S$-$T_+$ resonance, $\epsilon_S < \epsilon^*$. Since the time spent at the $S$-$T_+$ resonance during the pulse is short, the singlet is preserved with high probability. Next, detuning is brought back toward zero, to a value $\epsilon_F$, on a time scale slow compared to $T_2^*$ ($\sim 100$ ns). This converts $S$ to $T_+$ and flips a nuclear spin each cycle. Detuning is then rapidly moved to the point $M$ (again, over a time $\sim 1$ ns). While slightly different, both pulse sequences rely on bringing the $S$ and $T_+$ states into resonance; the otherwise large difference between nuclear and electron Zeeman energies would prevent flip-flop processes [23].

We begin by examining the statistical polarization sequence shown in Fig. 2(a). We first measure $P_S$ as a function of $B_0$ and $\epsilon_S$, with $\tau_S = 100$ ns, $\tau_P = 300$ ns, $\tau_{P'} = 100$ ns, $\tau_M = 32$ $\mu$s. These data, shown in Fig. 3(a), map out the $S$-$T_+$ anticrossing in the limit of minimal measurement induced polarization (polarization is negligible for $\tau_M > 30$ $\mu$s, as will be shown below). A steady-state nuclear polarization at $B_0 = 24$ mT results in a shift in the position of $\epsilon^*$, depending on the measurement time $\tau_M$, which determines the cycle period [Fig. 3(b)]. As $\tau_M$ decreases, the position of $\epsilon^*$ moves to larger values of detuning, indicating an increase in the average $B_{\text{nuc}}$. For $\tau_M > 30$ $\mu$s, the value of $\epsilon^*$ saturates to its unpolarized value. Values for $B_{\text{nuc}}(\tau_M)$ can be extracted from calibrat-
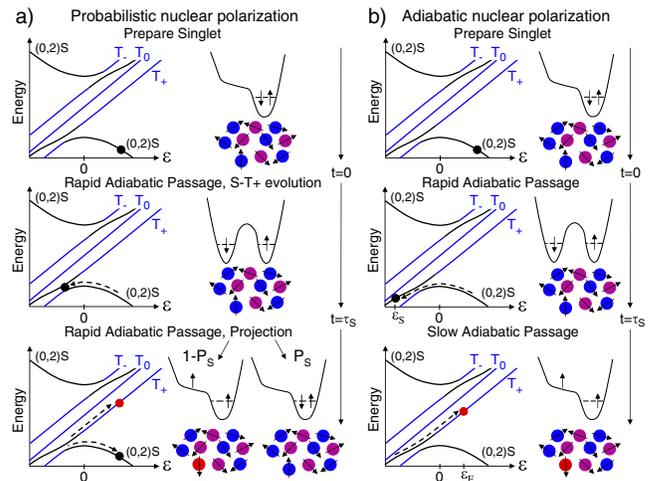
a)

b)



FIG. 2 (color online). (a) Probabilistic nuclear polarization sequence. (b) Adiabatic nuclear polarization sequence (see text).
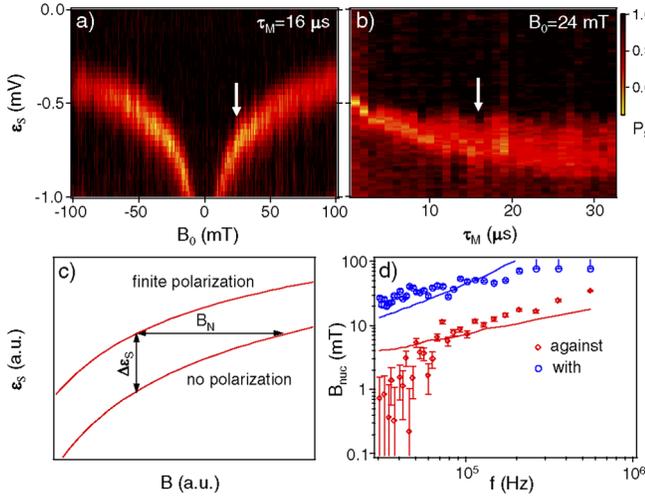
FIG. 3 (color online). (a) $P_S$ as a function of applied field $B_0$ and $\epsilon_S$. (b) Dependence of the $S$-$T_+$ anticrossing position on measurement duration $\tau_M$, with $B_0 = 24$ mT. A decrease in $\tau_M$ increases the polarization rate, shifting the $S$-$T_+$ resonance condition to more positive $\epsilon_S$. (c) Schematic diagram illustrating the effect of nuclear polarization on the spin funnel. $B_{\mathrm{nuc}}$ is extracted by measuring the shift in the $S$-$T_+$ position relative to the position without polarization. (d) $B_{\mathrm{nuc}}$ as a function of cycle frequency, $f$, measured sweeping $\epsilon_S$ to increasing values ("with") and decreasing values ("against"). Solid lines are predictions from a nonlinear diffusion model (see text).

ing the shift in $\epsilon^*$ using the data in Fig. 3(a), as illustrated in Fig. 3(c).

We find that both the position, $\epsilon^*$, and the width of the region where $P_S(\epsilon_S)$ is reduced below unity—marking the mean and fluctuations of the position of the $S$-$T_+$ anti-crossing—depend on the sweep direction used for data acquisition. In the present measurements, $\epsilon_S$ is swept on the inner loop, and $\tau_M$ is increased on the outer loop. Sweeping $\epsilon_S$ to more negative values [downward in Fig. 3(b)], i.e., *against* the movement of $\epsilon^*$ with increasing polarization, results in smaller nuclear polarization and a narrower resonance width compared to sweeping $\epsilon_S$ to more positive values (not shown), i.e., *with* the motion of $\epsilon^*$ as polarization builds up. The extracted $B_{\mathrm{nuc}}$ as a function of cycle frequency, $f = 1/(\tau_P + \tau_{P'} + \tau_S + \tau_M)$ is shown in Fig. 3(d) for the two sweep directions of $\epsilon_S$. In both cases, polarization increases with $f$ reaching a maximum value of $B_{\mathrm{nuc}} \sim 80$ mT [see Fig. 3(d)].

Qualitative features of the statistical DNP cycle [Fig. 2(a)] are accounted for by nonlinear rate equations for the nuclear polarization in the left and right dots, $P_{L,R}$. Within this model, a polarization-dependent probability per cycle of electron nuclear flip-flop, $p_{\mathrm{flip}}(P)$, where $P = P_L + P_R$ induces nuclear polarization, while out-diffusion relaxes polarization with rates $\Gamma_L$ and $\Gamma_R$ in the left and right dots. Nonlinearity arises from the dependence of $p_{\mathrm{flip}}$ on the distance $\Delta = \epsilon_S - \epsilon^*$ from the separation point to the anticrossing, which in turn depends on $B_{\mathrm{tot}}$, and hence

$P$. The relevant energy scale for $\Delta$ is the width of the $S$-$T_+$ anticrossing, $\Omega$. Writing $\Omega = \hbar\sqrt{2}\cos(\theta)/T_2^*$, where $\theta = \arctan(\frac{2t}{\epsilon_S - \sqrt{4|t|^2 + (\epsilon^*)^2}})$ is the adiabatic angle [24] that accounts for charge state mixing near $\epsilon = 0$, $T_2^*$ is the in-homogeneously broadened transverse relaxation time at the $S$-$T_+$ anticrossing, and $t$ is the interdot tunnel coupling, we find that the probability of a spin flip per cycle is given by $p_{\mathrm{flip}}(P) = [\Delta^2/(2\Omega^2) + 2]^{-1}$. Note that $p_{\mathrm{flip}} = 1/2$ at the anticrossing, $\epsilon_S = \epsilon^*$. Polarizations $P_L$, $P_R$ of the left and right dots then evolve according to coupled diffusion equations,

$$\frac{dP_{L,R}(t)}{dt} = -\Gamma_{L,R}P_{L,R} + \frac{p_{\mathrm{flip}}(P)fN_{L,R}}{3/2[N_L + N_R]^2}, \qquad (1)$$

where $N_L$ and $N_R$ are the number of nuclei in the left and right dots. The factor of $3/2$ reflects the spin-$3/2$ Ga and As nuclei. Results of the model using experimental parameters $N_L \sim N_R \sim 3 \times 10^6$, with $\Gamma = \Gamma_L + \Gamma_R$ as a fit parameter (assuming $\Gamma_L = \Gamma_R$), are shown in Fig. 3(d). The interdot tunnel coupling, $t/(g^*\mu_B) \sim 390$ mT, is determined from measurements of the charge occupancy as a function of detuning near the (1,1)-(0,2) interdot charge transition [25].

Qualitative agreement between experiment and model are seen in the dependence of polarization on cycle frequency and sweep direction. The fit gives $\Gamma \sim 0.3$ s$^{-1}$ which is consistent with out-diffusion predominantly perpendicular to the plane of the 2DEG, $\Gamma \sim D/d^2$, taking reasonable values for the electron gas thickness $d \sim 6$ nm and the nuclear diffusion constant $D \sim 10^{-13}$ cm$^2$/s [26]. Polarizations, $P_{\mathrm{nuc}} = B_{\mathrm{nuc}}/5.2$ T, exceeding the values of $\sim 1\%$ observed here can be achieved by increasing the cycle rate. Baugh *et al.* obtained polarizations approaching 20% in the Pauli blockade regime, which was associated with a tunneling rate of $10^8$ Hz, several orders of magnitude faster than the polarization cycle frequencies employed here [12]. In addition, nuclear polarizations of 60% have been achieved in self-assembled quantum dots using optical orientation [27].

We next investigate a self-limiting adiabatic DNP cycle that allows steady-state nuclear polarization to be set by a gate voltage, as illustrated in Fig. 2(b). The cycle is shown in terms of motion along energy levels in Fig. 4(a) and motion within the charge stability diagram in the inset of Fig. 4(c). The new feature in this sequence, compared to the statistical DNP cycle [Fig. 2(a)], is that the cycle passes *through* the anticrossing at $\epsilon^*$ quickly during the pulse to the separation point $\epsilon_S$, then slowly back to a point $\epsilon_F$, before moving quickly to the measurement point, $\epsilon_M$. The cycle then continues through $\epsilon_P$ and $\epsilon_{P'}$ as before. The position of $\epsilon_F$ is chosen so that at low polarization, it is to the right of $\epsilon^*$, as seen in the left diagram in Fig. 4(a). Adiabatic crossing of the $S$-$T_+$ anticrossing in the return direction results in a single electron-nuclear flip-flop and leads to nuclear polarization upon cycling. As polarization
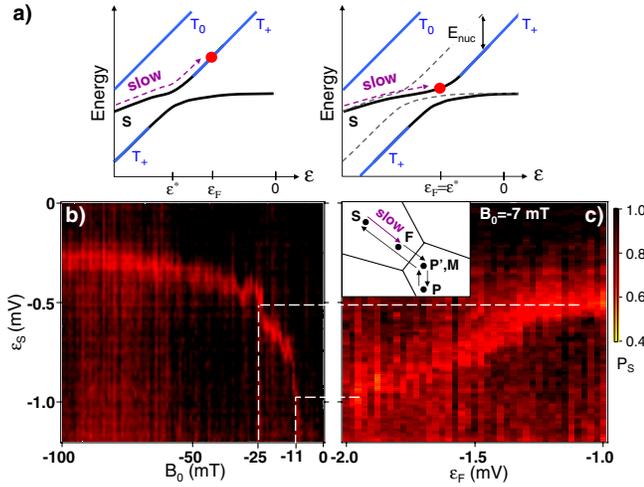
FIG. 4 (color online).   (a) Self-limiting adiabatic polarization sequence. Left: Starting with $B_{nuc} = 0$, the sequence polarizes nuclear spins and $B_{nuc}$ increases, shifting the $S$-$T_+$ resonance to more positive $\epsilon$. Right: Steady state is reached when $\epsilon^* = \epsilon_F$. Dashed gray lines show the energy level configuration before nuclear polarization. (b) Calibration spin funnel acquired using the pulse sequence [Fig. 1(c)]. (c) $P_S$ as a function of $\epsilon_F$ measured with the adiabatic polarization sequence applied. The complete pulse sequence consists of three adiabatic polarization cycles (a single adiabatic polarization cycle is shown in the inset) followed by one measurement cycle [shown in Fig. 1(c)]. The combined pulse sequence length is $\sim 6.4$ $\mu$s. Steady state hyperfine field $B_{nuc}$ changes from 4 to 18 mT as set-point $\epsilon_F$ is moved from $-2$ mV to $-1.3$ mV.

builds, $\epsilon^*$ moves to more positive values of detuning, until it coincides with the set-point, $\epsilon_F$, as illustrated on the right panel of Fig. 4(a). At that point, the buildup of polarization stops.

To both induce and measure a steady-state nuclear polarization, a sequence of three DNP cycles [Fig. 4(c), inset] followed by one measurement cycle [Fig. 1(c)] is iterated. We first calibrate changes in the position along $\epsilon$ with changes in $B_{nuc}$ by measuring $P_S$ as a function of $\epsilon_S$ and $B_0$, showing how $\epsilon^*$ depends on $B_{tot}$ in the absence of nuclear polarization [Fig. 4(b)]. Figure 4(c) shows that for the specific case of $B_0 = 7$ mT, the steady-state nuclear polarization can be controlled by the position of the set-point $\epsilon_F$, ranging from $B_{nuc} \sim 4$ mT for $\epsilon_F = -2$ mV to $B_{nuc} \sim 18$ mT for $\epsilon_F = -1.3$ mV. For $\epsilon_F > -1.3$ mV, $B_{nuc}$ saturates at $\sim 18$ mT. In these measurements, the low fields involved were necessary to allow calibration using plots like Fig. 4(a), which flatten and become insensitive to changes in $B_{nuc}$ at higher fields. This can be overcome by using single-electron spin resonance to calibrate $B_{nuc}$ at arbitrary fields [15,28]. Polarization with the adiabatic pulse sequence is less than expected given the

cycle rate (it should be twice as efficient as the probabilistic pulse sequence at a given cycle frequency, $f$) and did not grow when the cycle frequency was increased beyond the value used to acquire the data in Fig. 4(c). Further experiments are required to determine if dark state formation is limiting polarizations obtained with this pulse sequence, where successive interactions at the $S$-$T_+$ degeneracy take place on $\sim 300$ ns time scales, which are much shorter than nuclear spin decoherence times [23].

[1] L. P. Kouwenhoven *et al.*, in *Mesoscopic Electron Transport*, edited by L. P. Kouwenhoven, G. Schön, and L. L. Sohn (Kluwer, Dordrecht, 1997).
[2] R. Hanson *et al.*, Rev. Mod. Phys. **79**, 1217 (2007).
[3] G. Chen, D. L. Bergman, and L. Balents, Phys. Rev. B **76**, 045312 (2007).
[4] W. A. Coish *et al.*, J. Appl. Phys. **101**, 081715 (2007).
[5] H. Christ, J. I. Cirac, and G. Giedke, Phys. Rev. B **75**, 155324 (2007).
[6] M. S. Rudner and L. S. Levitov, arXiv:0705.2177.
[7] K. Wald *et al.*, Phys. Rev. Lett. **73**, 1011 (1994).
[8] G. Yusa *et al.*, Nature (London) **434**, 1001 (2005).
[9] K. Ono *et al.*, Science **297**, 1313 (2002).
[10] F. H. L. Koppens *et al.*, Science **309**, 1346 (2005).
[11] K. Ono and S. Tarucha, Phys. Rev. Lett. **92**, 256803 (2004).
[12] J. Baugh *et al.*, Phys. Rev. Lett. **99**, 096804 (2007).
[13] A. C. Johnson *et al.*, Nature (London) **435**, 925 (2005).
[14] J. R. Petta *et al.*, Science **309**, 2180 (2005).
[15] F. H. L. Koppens *et al.*, Nature (London) **442**, 766 (2006).
[16] S. I. Erlingsson, Y. V. Nazarov, and V. I. Falko, Phys. Rev. B **64**, 195306 (2001).
[17] A. V. Khaetskii, D. Loss, and L. Glazman, Phys. Rev. Lett. **88**, 186802 (2002).
[18] D. Klauser, W. A. Coish, and D. Loss, Phys. Rev. B **73**, 205302 (2006).
[19] D. Stepanenko *et al.*, Phys. Rev. Lett. **96**, 136401 (2006).
[20] J. M. Taylor, C. M. Marcus, and M. D. Lukin, Phys. Rev. Lett. **90**, 206803 (2003).
[21] M. V. G. Dutt *et al.*, Science **316**, 1312 (2007).
[22] D. Paget, G. Lampel, and B. Sapoval, Phys. Rev. B **15**, 5780 (1977).
[23] A. Imamoglu *et al.*, Phys. Rev. Lett. **91**, 017402 (2003).
[24] J. M. Taylor *et al.*, Phys. Rev. B **76**, 035315 (2007).
[25] L. DiCarlo *et al.*, Phys. Rev. Lett. **92**, 226801 (2004).
[26] D. Paget, Phys. Rev. B **25**, 4444 (1982).
[27] A. S. Bracker *et al.*, Phys. Rev. Lett. **94**, 047402 (2005).
[28] E. A. Laird *et al.*, Phys. Rev. Lett. **99**, 246601 (2007); K. C. Nowack *et al.*, Science **318**, 1430 (2007).